Video-based biomechanical analysis of an unexpected Achilles tendon rupture in an Olympic sprinter

Irineu Loturco[1,2,3], Carlos De la Fuente[4,5,6], Chris Bishop[7], Hélio Nichioka[8], Denise Lessio[8], Carlos T. Moreno[9], Lucas A. Pereira[1,2], Felipe P. Carpes[4,*]

1 - Nucleus of High Performance in Sport, São Paulo, Brazil

2 - Department of Human Movement Sciences, Federal University of São Paulo, São Paulo, Brazil

3 - University of South Wales, Pontypridd, Wales, United Kingdom

4 - Applied Neuromechanics Research Group, Universidade Federal do Pampa, Uruguaiana, RS, Brazil

5 - Carrera de Kinesiología, Departamento de Cs. de la Salud, Facultad de Medicina, Pontificia Universidad Católica, Santiago, Chile

6 - Centro de Salud Deportivo, Clinica Santa Maria, Santiago, Chile

7 - Faculty of Science and Technology, London Sports Institute, Middlesex University, London, UK

8 - Instituto Nichioka, São Paulo, Brazil

9 - Department of Orthopedics and Traumatology, Federal University of São Paulo (Unifesp), São Paulo, SP, Brazil

*** Corresponding author:** Felipe P Carpes, Ph.D. Postal address: Federal University of Pampa - Laboratory of Neuromechanics, PO box 118 - ZIP 97501-970, Uruguaiana, RS, Brazil. Phone office: +55 55 3911 0225; e-mail: carpes@unipampa.edu.br

Abstract

We used image-processing techniques to determine the moment (i.e., image frame) of the Achilles tendon (AT) rupture in an Olympic sprinter. This report may be unique due to the difficulty in conducting motion capture analyses during injury events. Our report includes one female Olympic sprinter, 29 years old (body mass: 56 kg, height: 1.68 m, and body mass index: 19.8 kg/m^2) with a high-competitive profile history (2008 and 2012 Olympic Games participation; South American record holder in 100- and 200-m; Pan-American gold medalist in 200-m and 4 x 100-m relay) who suffered a complete AT rupture in the left leg while exercising in the final phase of rehabilitation following an Achilles tendinopathy in the contralateral limb. The greater dorsiflexion found at the moment of the injury and the delayed control of heel position indicated the presence of uncontrolled dorsiflexion, which potentially generated excessive eccentric stress over the tendon and, thus, the AT rupture. Here we discuss the relevance of lower leg alignment, the movements' characteristics, and the history of Achilles tendinopathy in the contralateral leg on the occurrence of the AT rupture.

Keywords: Tendon injuries; Kinematics; Sprint; Jumping.

Introduction

Push-off and weight-bearing actions, sudden, and forced dorsiflexion during fast and powerful activities involving acceleration and deceleration of the body's center of mass are conditions that increase the risk of an Achilles tendon (AT) rupture in elite sports (Hess, 2010). When a rupture occurs, biomechanical analyses of movement are valuable to identify and examine mechanisms that could lead to this traumatic event. Nevertheless, biomechanical examination of an unexpected AT rupture is very difficult to conduct, since it requires motion capture during the injury event. Our objective is to identify (using the image analysis) the exact time of an acute and unexpected complete AT rupture in an Olympic female sprinter.

Methods

This report includes one female Olympic sprinter, 29 years old (body mass: 56 kg, height: 1.68 m, and body mass index: 19.8 kg/m^2) with a high-competitive profile history (2008 and 2012 Olympic Games participation; South American record holder in 100- and 200-m; Pan-American gold medalist in 200-m and 4 x 100-m relay) who suffered a complete AT rupture in the left leg while exercising in the final phase of the rehabilitation period (see the video recording in supplementary file 1). She was preparing to return to sprint training after 10 weeks of treatment for an AT injury classified as a “chronic tendinopathy” in the contralateral lower limb (i.e., her preferred leg). The rupture occurred 40 minutes after the start of a session consisting of three parts: 1) 15-min warm up (e.g., active stretching and running at moderate intensity), 2) 6-8 sets of 6-8 repetitions of functional sprint drills (e.g., skipping and hopping exercises), and 3) 6-8 sets of 6-8 repetitions of unilateral and bilateral plyometric jumps (e.g., drop jumps). Rupture happened during the third part of the session and was confirmed by image exams (see supplementary file 2). The athlete did not report any pain or symptoms related to the injury prior to the event. The moment of the rupture was recorded because the training sessions were regularly documented throughout the rehabilitation period. From the captured video, we used image-processing techniques to determine the moment (i.e., image frame) of the AT rupture. This study was conducted according to the Declaration of Helsinki and the athlete gave consent to share the data for this report, including the videos and all associated MRI images.

Data Analysis

Digital image processing was conducted to identify the instant when the AT rupture occurred during the stance phase of landing while performing a bilateral drop jump, considering a methodological approach similar to a previous study (De la Fuente et al., 2019). We also included a comparative analysis of a similar jump performed in the same session, before the AT rupture. Video was recorded at 240 Hz by a smartphone (iPhone 7, Apple Inc., Cupertino, CA, USA) placed approximately one meter behind the movement.

*** Figure 1 near here please ***

To identify the moment of the rupture, we considered the abrupt changes in the leg skin shape (De la Fuente et al., 2019). We determined the image centroid (geometric barycenter) to quantify the changes in muscle shape due to the AT rupture and the consequent rapid muscle retraction in the injured leg. The centroid was equal to $\frac{\sum_{i,j} I_{i,j} \begin{bmatrix} i \\ j \end{bmatrix}}{\sum_{i,j} I_{i,j}}$, where $I_{i,j}$ is the intensity of the segmented pixels (McManus et al., 2011). The horizontal and vertical trajectories of the centroid were normalized to the first frame of the ruptured AT sequence. Each image was converted to YCbCr luminance - chrominance space to find the best skin segmentation (highest sensibility and lowest 1-specificity). The best segmentation was defined by changing Cb and Cr parameters from the region of interest (RoI) via the search grid (see Table 1). We obtained the true positive (TP), which was the number of pixels correctly classified as skin; the false negative (FN), which was the number of pixels wrongly classified as no skin when they represented skin (type II error); the true negative (TN), which was the number of pixels correctly classified as no skin; and false positive (FP), which was the number of pixels wrongly classified as skin when they were no skin (Type I error), see Table 1.

*** Table 1 near here please ***

The RoI was manually identified in the injured leg considering knee and malleolus line references (see Figure 2 for details of the steps). This step was manual because it is clearly possible to identify the injured leg, and an automatic recognition of the leg would cost more processing time to the data. The segmentation was performed from malleolus to the knee level by the same researcher.

The researchers also conducted a test-retest of centroid determination considering each frame (Table 2). All-time series for the ruptured and a non-ruptured jump were time-normalized, from 0 to 100%. The average values were considered.

*** Figure 2 near here please ***

*** Table 2 near here please ***

To detect anomaly between the time series, the square error difference between detrended ruptured and non-ruptured trajectories were defined using the Grubb Test, which was utilized to identify the most probable frame where the total rupture happened considering the outlier frame using α = 0.05. The Grub test was developed for detecting the largest anomaly within a univariate sample set, where H_0 established that there are no outliers within the data set (Cohn et al., 2013; Hochenbaum et al., 2017). The statistic of Grub test is defined by $\mathrm{C} = \frac{max|xt-\bar{x}|}{\sigma}$, and to reject the H_0 at significance level, α is defined by $\mathrm{C} > \frac{(N-1)}{\sqrt{N}}\sqrt{\frac{{t_{\alpha/(2N,N-2)}}^2}{N-2+{t_{\alpha/(2N,N-2)}}^2}}$ (Hochenbaum et al., 2017).

Additionally, the ankle movement was estimated during the stance phase of the respective video. We were unable to perform the same analysis in the non-ruptured video because in this video the rearfoot is not clearly seen. To conduct this analysis, we considered the tip of the left shoe, the center of posterior left shoe, and the center of the posterior aspect of knee in the video where the AT rupture occurred. Finally, the ankle movement (maximum value) allowed us to estimate the absorption (dorsiflexion) and propulsion (plantar flexion) phases. All procedures were performed using the Matlab 2016a software (Mathworks, Inc., USA).

Results

The muscle contour of the medial gastrocnemius suffered a sudden change of position due to the mechanic energy released after the AT rupture (Figure 1, frame 12, and see also the supplementary video). After anomaly detection, we determined that the rupture happened at 58% of the stance phase (absorption phase) with $p < 0.05$ (Figure 3A-C). The larger centroid displacement in the x-coordinate was identified at 74% with $p < 0.05$.

Regarding the tuning parameters for skin area segmentation, the best leg shape fit was found for Cb = 90 to 130, and for Cr = 135 to 165 (Figure 2). The sensibility obtained was 0.99, and the 1-specificity was 0.07. Regarding the reliability of this automated method to obtain the centroid, we found a high reliability for the jump with and without the AT rupture (see Table 2).

*** Figure 3 near here ***

Discussion

We conducted a biomechanical analysis of an acute AT rupture in a female Olympic sprinter considering the information from a video recorded during a jump exercise. This is one of the few reports considering an actual injury condition that comprises a biomechanical analysis to discuss the injury causes and characteristics. The elevated dorsiflexion at the moment of the rupture, which was greater than expected for weight-bearing movements (Rabin et al., 2015), and the delayed control of heel position, suggested the presence of an uncontrolled dorsiflexion during the absorption phase, together with a forced tendon elongation generating an excessive stress over the tendon support the occurrence of an eccentric muscle action in the moment of the rupture (De la Fuente et al., 2019). Insufficient muscle activation both at ankle (increasing dorsiflexion) and/or knee (increasing extension) joints prior to the weight bearing may explain the uncontrolled dorsiflexion, in which the poor coordination between knee-ankle coordination can predispose to AT rupture (De la Fuente et al., 2019).

The plyometric task performed involved sudden acceleration and deceleration of the body center of mass, which are recognized as risk factors for AT ruptures (Chiodo and Wilson, 2006; Hess, 2010). The greater tendon elongation likely increased the mechanical stress at the mid-substance zone (Shim et al., 2014), and possibly explains the AT rupture identified at the mid-substance zone. In the case of degeneration in the mid-substance zone, increased tension might not be necessary to cause AT failure (Thomopoulos et al., 2015). We were not able to determine whether the athlete showed signs of degeneration in the mid-substance zone, as well as to fully describe the training routine before the injury. However, we know that at the moment of the injury, the athlete did not report any symptoms that could indicate an imminent risk for a prospective AT rupture, especially on the contralateral side.

The larger elongation of AT with increased dorsiflexion may suggest impaired muscle coordination or co-activation of extensor muscles. This condition may be a result of intra-session cumulative fatigue due to repetitive eccentric loads, which are related to excitation-couple dysfunction, shift in optimal length-tension relationships, rise in passive tension, and decrease in maximal voluntary contraction (Proske and Morgan, 2001). It is also possible that some degree of fatigue due to previous training may have influenced some neurophysiological mechanisms associated with lower limb movement (Gandevia, 2001). The rupture occurred 40 minutes after the beginning of the activity, and it is possible to speculate that some degree of muscle fatigue in the injured limb may have contributed to the AT rupture, since fatigue may change muscle recruitment and inhibit the proper functionality of α-motor neurons (MacIntosh et al., 2012). It can also alter work distribution between the joints (Barbieri et al., 2014) and has been previously shown to increase ground reaction forces during landing tasks (Thomas et al., 2010).

Knee hyperextension, and ankle and subtalar joints kinematics in the frontal plane are other factors that could be considered when discussing the characteristics of the rupture. However, we were unable to conduct a three-dimensional analysis due to the nature of the video recorded. The combination of reduced dorsiflexion and knee extension is suggested as a risk factor for AT injury (Kaufman et al., 1999). Runners with AT tendinopathy showed increased eversion during running (Donoghue et al., 2008; Kulig et al., 2011), and the excessive pronation of subtalar suggest increased strain of the medial fibers of the AT during stance, a phenomenon called “whipping” or “bowstring” effect (Kulig et al., 2011; Ryan et al., 2009). Comparing the movements from the video including the AT rupture with the video before the rupture, it is possible to note that, at the traumatic moment, the sprinter presented an increased ankle eversion, accompanied by excessive dynamic valgus and knee hyperextension. These movements may contribute to overload the medial gastrocnemius and increase AT elongation and may also be a symptom of muscle fatigue. Previous experiments suggest that the fatigue of plantar flexors (Bobbert et al., 2011) and quadriceps alters the knee-ankle inter-limb coordination during jump tasks (Rodacki et al., 2002). However, we were unable to quantify these movements through the captured images.

Our analysis is limited to a two-dimensional assessment. A three-dimensional approach was not possible, but it could contribute to reinforce our findings. To discuss the movement characteristics after determining the moment of the rupture it was considered the best comparable jump performed within the same training session, but we acknowledge that the visual inspection of the same movement at a second position, ideally in the sagittal plane, would permit a more detailed and precise discussion of this case (Souza, 2016). However, a detailed and consistent methodology (i.e. image processing, validity, and reliability analyses) was employed to extract the most usable information possible for our discussion and inferences.

Conclusions

The AT rupture in the female Olympic sprinter occurred at 58% of the stance phase before the beginning of the push-off, thus characterizing an eccentric rupture. We believe that an uncontrolled dorsiflexion, as suggested by the greater dorsiflexion and delayed control of heel position, may have accounted for the AT rupture. An excessive eccentric stress over the AT and a stretched gastrocnemius seem to also contribute to the AT rupture. The influence of technique on injury risk factors during sport-specific activities highlights the need for specific motion analysis routines during the recovery processes of elite athletes.

References

Barbieri, F.A., Gobbi, L.T., Lee, Y.J., Pijnappels, M., van Dieen, J.H., 2014. Effect of triceps surae and quadriceps muscle fatigue on the mechanics of landing in stepping down in ongoing gait. Ergonomics 57, 934-942.

Bobbert, M.F., van der Krogt, M.M., van Doorn, H., de Ruiter, C.J., 2011. Effects of fatigue of plantarflexors on control and performance in vertical jumping. Med Sci Sports Exerc 43, 673-684.

Chiodo, C.P., Wilson, M.G., 2006. Current concepts review: acute ruptures of the achilles tendon. Foot Ankle Int 27, 305-313.

Cohn, T.A., England, J.F., Berenbrock, C.E., Mason, R.R., Stedinger, J.R., Lamontagne, J.R., 2013. A generalized Grubbs‐Beck test statistic for detecting multiple potentially influential low outliers in flood series. Water Resources Research, 5047–5058.

De la Fuente, C., Ramirez-Campillo, R., Gallardo-Fuentes, F., Alvarez, C., Bustamante, C., Henriquez, H., Carpes, F.P., 2019. Pattern analysis of a complete Achilles tendon rupture suffered during high jump preparation in an official national-level athletic competition. Sports Biomech, 1-11.

Donoghue, O.A., Harrison, A.J., Laxton, P., Jones, R.K., 2008. Lower limb kinematics of subjects with chronic achilles tendon injury during running. Res Sports Med 16, 23-38.

Gandevia, S.C., 2001. Spinal and supraspinal factors in human muscle fatigue. Physiol. Rev. 81, 1725–1789.

Hess, G.W., 2010. Achilles tendon rupture: a review of etiology, population, anatomy, risk factors, and injury prevention. Foot & ankle specialist 3, 29-32.

Hochenbaum, J., Owen, S., Vallis, A.K., 2017. Automatic Anomaly Detection in the Cloud Via Statistical Learning, arXiv.org. Cornell University, p. 13.

Kaufman, K.R., Brodine, S.K., Shaffer, R.A., ohnson, C.W., Cullison, T., 1999. The effect of foot structure and range of motion on musculoskeletal overuse injuries. Am J Sports Med 27, 585-593.

Kulig, K., Loudon, J.K., Popovich, J.M., Pollard, C.D., Winder, B.R., 2011. Dancers with achilles tendinopathy demonstrate altered lower extremity takeoff kinematics. J Orthop Sports Phys Ther 41, 606-613.

MacIntosh, B.R., Holash, R.J., Renaud, J.M., 2012. Skeletal muscle fatigue-regulation of excitation-contraction coupling to avoid metabolic catastrophe. J. Cell. Sci. 125, 2105–2114.

McManus, I.C., Stöver, K., Kim, D., 2011. Arnheim's Gestalt theory of visual balance: Examining the compositional structure of art photographs and abstract images. Iperception 2, 615-647.

Proske, U., Morgan, D.L., 2001. Muscle damage from eccentric exercise: mechanism, mechanical signs, adaptation and clinical applications. J. Physiol. (Lond.) 537, 333–345.

Rabin, A., Kozol, Z., Spitzer, E., Finestone, A.S., 2015. Weight-bearing ankle dorsiflexion range of motion-can side-to-side symmetry be assumed? J Athl Train 50, 30-35.

Rodacki, A.L., Fowler, N.E., Bennett, S.J., 2002. Vertical jump coordination: fatigue effects. Med Sci Sports Exerc 34, 105-116.

Ryan, M., Grau, S., Krauss, I., Maiwald, C., Taunton, J., Horstmann, T., 2009. Kinematic analysis of runners with achilles mid-portion tendinopathy. Foot Ankle Int 30, 1190-1195.

Shim, V.B., Fernandez, J.W., Gamage, P.B., Regnery, C., Smith, D.W., Gardiner, B.S., Lloyd, D.G., Besier, T.F., 2014. Subject-specific finite element analysis to characterize the influence of geometry and material properties in Achilles tendon rupture. J Biomech 47, 3598-3604.

Souza, R.B., 2016. An Evidence-Based Videotaped Running Biomechanics Analysis. Phys Med Rehabil Clin N Am 27, 217-236.

Thomas, A.C., McLean, S.G., Palmieri-Smith, R.M., 2010. Quadriceps and hamstrings fatigue alters hip and knee mechanics. J Appl Biomech 26, 159-170.

Thomopoulos, S., Parks, W.C., Rifkin, D.B., Derwin, K.A., 2015. Mechanisms of tendon injury and repair. J Orthop Res 33, 832-839.

Figures captions

Figure 1. All consecutive frames included in the analysis of stance phase when the AT rupture happened. Highlighted is the frame when the AT rupture was detected (12th frame). A sudden reduction in gastrocnemius area and retraction of the muscle belly is observed in the video. The grayscale bar represents the intensity value of pixels, where 0 is black and 255 is white. Further details can be seen in the supplemental video.

Figure 2. Centroid estimation from the leg skin. A shows the raw image. B shows the skin segmentation by luminescence (YCbCr) for the overall image. C shows the manual definition of the region of interest in the injured leg. D shows the skin segmentation in the injured leg. C shows the localization of the centroid in the segmented leg.

Figure 3. Identification of the moment when Achilles tendon (AT) rupture happens during the stance phase from a bilateral drop jump and a comparison with a bilateral drop without AT rupture. A shows the ankle kinematics (dorsiflexion – plantar flexion). B shows the horizontal displacement of the skin leg centroid normalized to the horizontal range of leg skin. C shows the vertical displacement of skin leg centroid normalized to the vertical range of leg skin. D shows the square error of detrended centroid $[\text{centroid}_{\text{x-with AT rupture}} - \text{centroid}_{\text{x-with AT rupture}}]^2$ between the jump with and without the AT rupture. E shows the square error of detrended centroid $[\text{centroid}_{\text{y-with AT rupture}} + \text{centroid}_{\text{y-with AT rupture}}]^2$ between the jumps. Absorption and propulsion (prop) phases are indicated only for the AT rupture jump. * indicates a p-value < 0.05 for the Grubb test, which means that a statistical maximal outlier exists and indicates the moment of the AT rupture.

Table 1. Skin segmentation of YCbCr color space. Number of pixels classified as skin or no skin for luminescence parameters Cb and Cr using different lengths of parameters by grid search.

Length of parameters	Parameters		True Positive	False Negative	True Negative	False Positive	Sensibility	1-Specificity
	Cb	Cr						
20	100-120	130-150	5986	929	157693	6753	0.87	**0.04**
	100-120	140-160	5716	1199	158541	5905	0.83	**0.04**
	110-130	130-150	6784	131	147873	16573	**0.98**	0.10
	110-130	140-160	5850	1065	159188	5258	0.85	**0.03**
30	90-120	120-150	5986	929	156938	7508	0.87	**0.05**
	90-120	130-160	6103	812	156174	8272	0.88	**0.05**
	90-120	140-170	5716	1199	157489	6957	0.83	0.04
	100-130	120-150	6798	117	103584	60862	**0.98**	0.37
	100-130	130-160	6914	1	146278	18168	1.00	0.11
	100-130	140-170	5881	1034	157928	6518	0.85	0.04
	110-140	120-150	6785	130	10638	153808	**0.98**	0.94
	110-140	130-160	6883	32	146318	181128	**1.00**	0.11
	110-140	140-170	5850	1065	158801	5645	0.85	**0.03**
40	80-120	110-150	5986	929	156577	7869	0.87	**0.05**
	80-120	120-160	6103	812	155371	9075	0.88	0.06
	80-120	130-170	6103	812	154476	9970	0.88	0.06
	80-120	140-180	5716	1199	156432	8014	0.83	**0.05**
	90-130	110-150	6798	117	102915	61531	**0.98**	0.37
	90-130	120-160	6915	0	102019	62427	**1.00**	0.38
	90-130	130-170	6914	1	145037	19409	**1.00**	0.12
	90-130	140-180	5881	1034	156904	7542	0.85	0.05
	100-140	110-150	6798	117	8111	156335	**0.98**	0.95
	100-140	120-160	6915	0	8873	155573	**1.00**	0.95
	100-140	130-170	6914	1	144827	19619	**1.00**	0.12
	100-140	140-180	5881	1034	157567	6879	0.85	**0.04**
	110-150	110-150	6785	130	8222	156224	**0.98**	0.95
	110-150	120-160	6884	31	10124	154322	**1.00**	0.94
	110-150	130-170	6883	32	146246	18200	**1.00**	0.11
	110-150	140-180	5850	1065	158801	5645	0.85	**0.03**
50	70-120	100-150	5986	929	156492	7954	0.87	**0.05**
	70-120	110-160	6103	812	155208	9238	0.88	0.06
	70-120	120-170	6103	812	153975	10471	0.88	0.06
	70-120	130-180	6103	812	154277	10169	0.88	0.06
	70-120	140-190	5716	1199	156273	8173	0.83	**0.05**
	80-130	100-150	6798	117	102554	61892	**0.98**	0.38
	80-130	110-160	6915	0	101326	63120	**1.00**	0.38
	80-130	120-170	6915	0	100321	64125	**1.00**	0.39
	80-130	130-180	6914	1	143849	20597	**1.00**	0.13
	80-130	140-190	5881	1034	155847	8599	0.85	**0.05**
	90-140	100-150	6798	117	7633	156813	**0.98**	0.95
	90-140	110-160	6915	0	6461	157985	**1.00**	0.96
	90-140	120-170	6915	0	7587	156859	**1.00**	0.95
	90-140	130-180	6914	1	143614	20832	**1.00**	0.13
	90-140	140-190	5881	1034	156543	7903	0.85	**0.05**
	100-150	100-150	6798	117	7171	157275	**0.98**	0.96
	100-150	110-160	6915	0	6457	157989	**1.00**	0.96
	100-150	120-170	6915	0	8548	155898	**1.00**	0.95
	100-150	130-180	6914	1	147802	16644	**1.00**	0.04
	100-150	140-190	5881	1034	157567	6879	0.85	**0.04**
	110-160	100-150	6785	130	7899	156547	**0.98**	0.95
	110-160	110-160	6884	31	7869	156577	**1.00**	0.95
	110-160	120-170	6884	31	10076	154370	**1.00**	0.94
	110-160	130-180	6883	32	146246	18200	**1.00**	0.11
	110-160	140-190	5850	1065	158801	5645	0.85	**0.03**

Only sensibility > 0.70 were included in the table.
Sensibility ≥ 0.95 and 1-Specificity ≤ 0.05 in bold

True positive (TP): number of pixels correctly classified as skin.
False negative (FN): number of pixels wrongly classified as no skin when they were skin (type II error).
True negative (TN): number of pixels correctly classified as no skin.
False positive (FP): number of pixels wrongly classified as skin when they were no skin (type I error).
Sensibility: the ability to detect skin [TP / (TP + FN)].
Specificity: the ability to detect non-skin [TN / (TN + FP)].

Table 2. Intra-class correlation coefficients found for twenty repetitions (n=20) of algorithm application by same researcher for each video. The table shows the reliability of parameters chosen (Cb = 90 to 130 and Cr = 135 to 165) to segmented skin.

	n	**Coefficient**	**95% Confidence Interval**		***p*-value**
			Lower bound	**Upper bound**	
Jump with AT rupture					
Centroid_y	20	0.978	0.961	0.990	<0.001
Centroid_x	20	0.998	0.996	0.999	<0.001
Jump without AT rupture					
Centroid_y	20	0.998	0.992	1.000	<0.001
Centroid_x	20	0.925	0.727	0.995	<0.001

Ho : ICC = 0 (F-Test).
AT: Achilles tendon

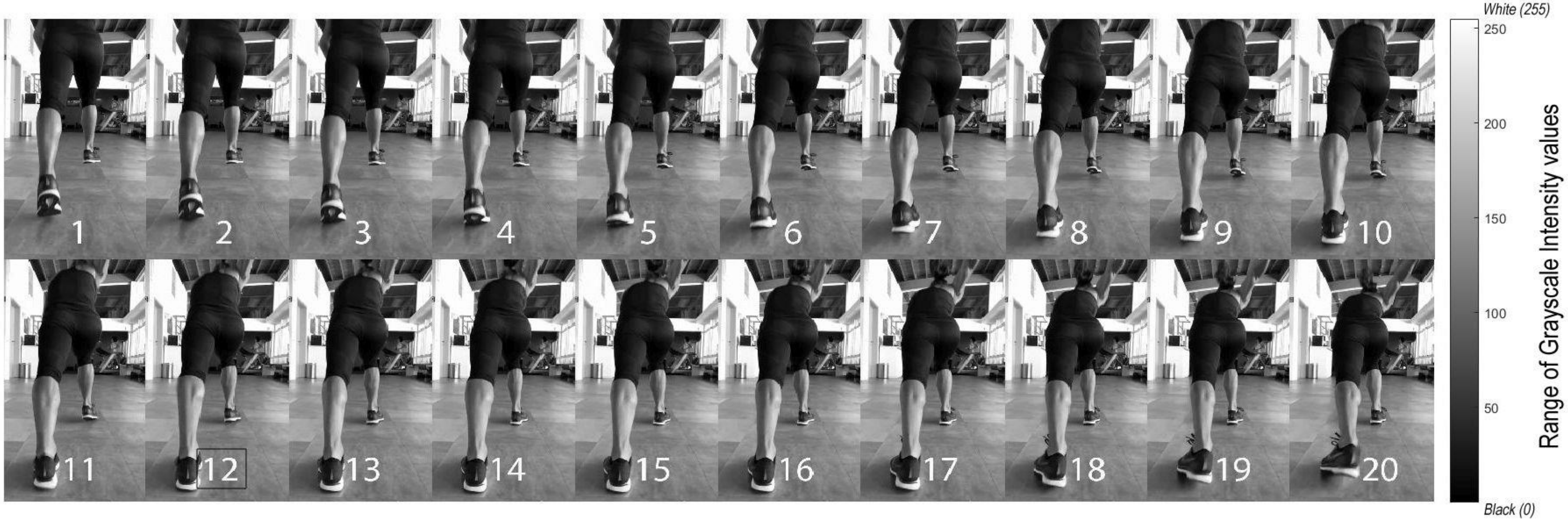
1
2
3
4
5
6
7
8
9
10
11
12
13
14
15
16
17
18
19
20
White (255)
250
200
150
100
50
Black (0)
Range of Grayscale Intensity values

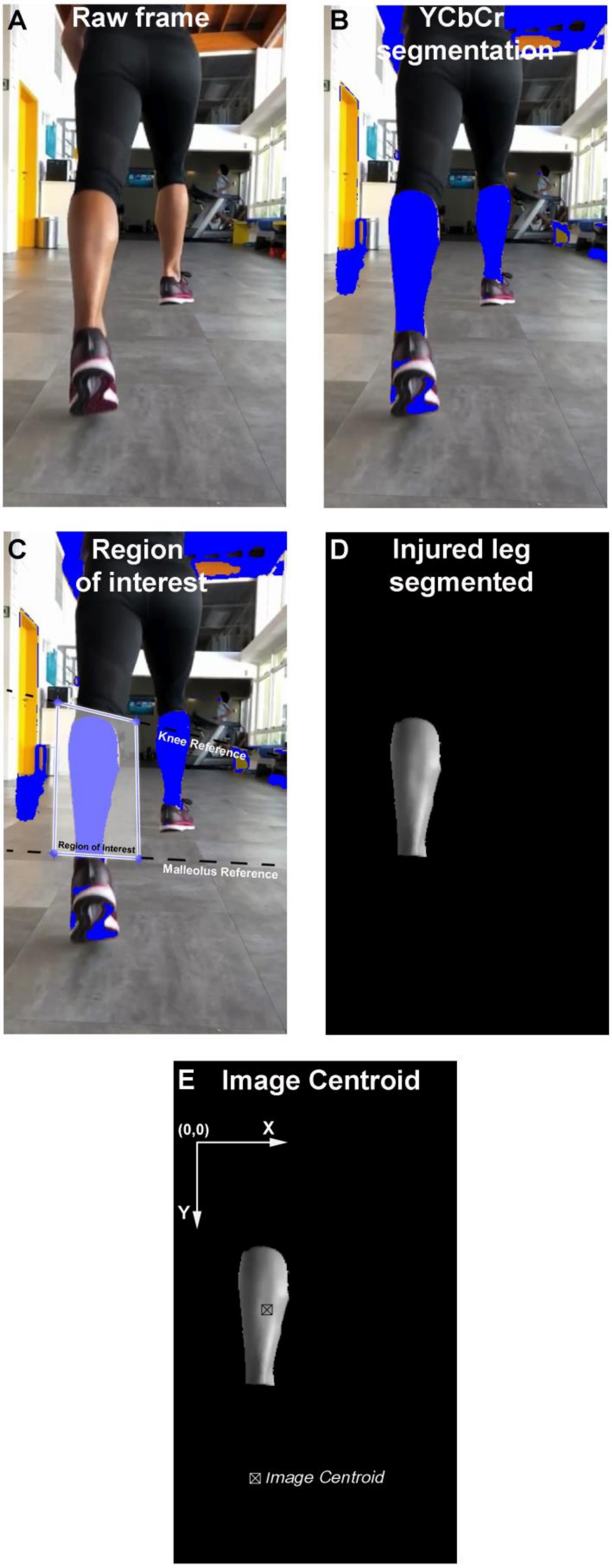
A
Raw frame
B
YCbCr segmentation
C
Region of interest
Knee Reference
Region of Interest
Malleolus Reference
D
Injured leg segmented
E
Image Centroid
(0,0)
X
Y
⊠ Image Centroid

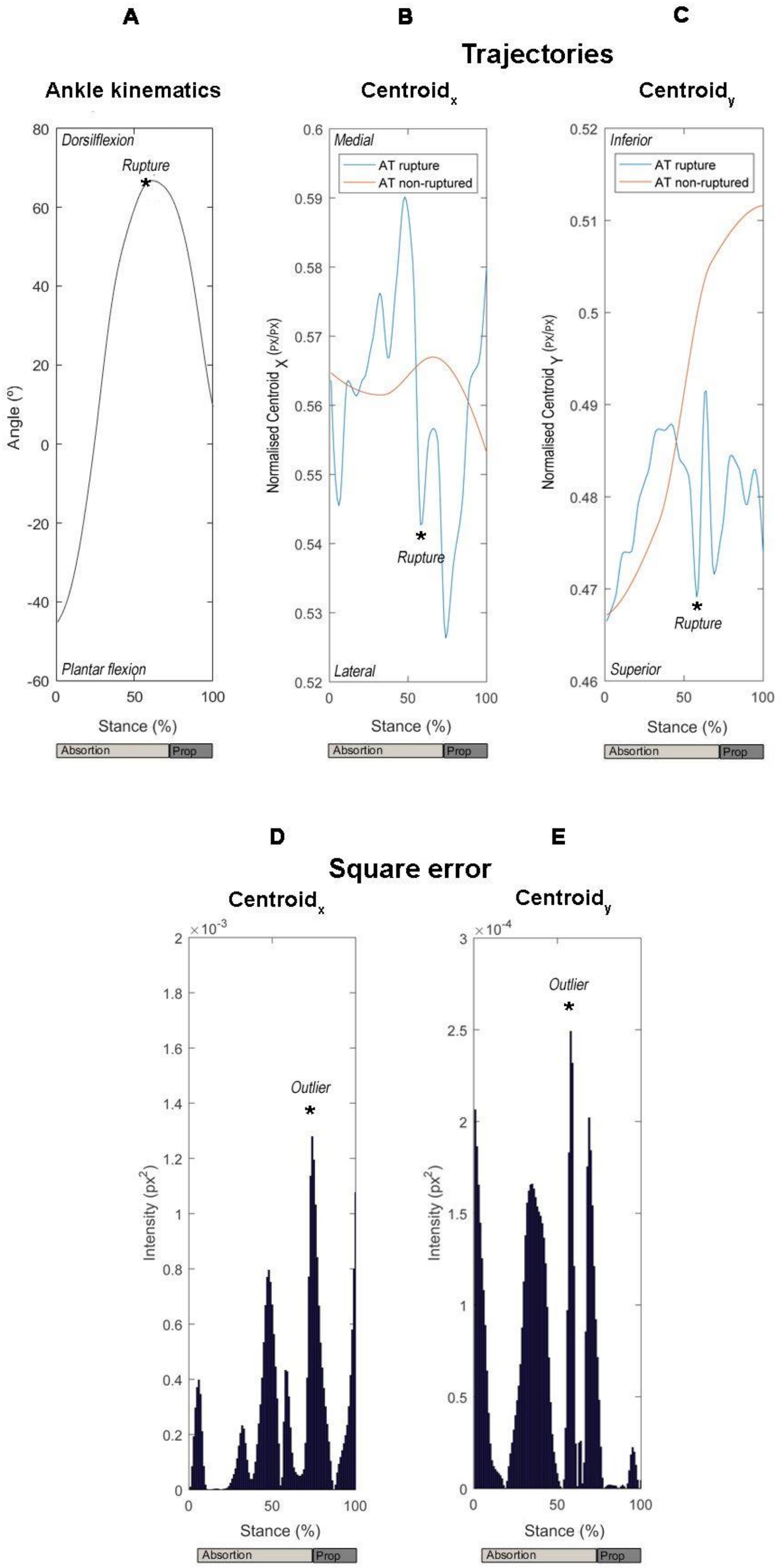
A
B
C
Trajectories
Ankle kinematics
Centroid$_x$
Centroid$_y$
Dorsiflexion
Rupture
Plantar flexion
Angle (º)
80
60
40
20
0
-20
-40
-60
Stance (%)
0
50
100
Absortion
Prop
Medial
Lateral
AT rupture
AT non-ruptured
Normalised Centroid X (PX/PX)
0.6
0.59
0.58
0.57
0.56
0.55
0.54
0.53
0.52
Rupture
Inferior
Superior
Normalised Centroid Y (PX/PX)
0.52
0.51
0.5
0.49
0.48
0.47
0.46
Rupture
D
E
Square error
Centroid$_x$
Centroid$_y$
$\times 10^{-3}$
2
1.8
1.6
1.4
1.2
1
0.8
0.6
0.4
0.2
0
Intensity (px^2)
Outlier
$\times 10^{-4}$
3
2.5
2
1.5
1
0.5
0
Outlier
Stance (%)
Absortion
Prop